ACS Catalysis

RESEARCH ARTICLE

pubs.acs.org/acscatalysis

Synthesis and Characterization of Cluster-Derived $PtRu_5Sn$ Catalysts

Karen J. Uffalussy,[†] Burjor K. Captain,[‡] Richard D. Adams,[‡] Ana B. Hungria,[§] John R. Monnier,[†] and Michael D. Amiridis*[,†]

[†]Department of Chemical Engineering, [‡]Department of Chemistry and Biochemistry, University of South Carolina, Columbia, South Carolina 29208, United States

[§]Department of Chemistry, University of Cadiz, 11001 Cadiz, Spain

ABSTRACT: Magnesia-supported trimetallic Pt−Ru−Sn catalysts prepared through a cluster and a conventional synthetic route have been investigated in terms of their structural properties and their catalytic activity for the hydrogenation of citral. FTIR results indicate that the majority of the stabilizing ligands remain attached to the $PtRu_5(\mu\text{-}SnPh_2)(C)(CO)_{15}$ cluster used following impregnation onto the MgO support. Under H_2 reduction conditions, partial and full ligand removal are observed at 473 and 573 K, respectively. HRSTEM analysis shows that cluster-derived samples exhibit significantly smaller average metal particle sizes, as well as narrower particle size distributions than the corresponding conventionally prepared ones. EDS measurements show that in the cluster-derived catalysts, the majority of the metal particles present are trimetallic in nature, with metal compositions similar to those of the original cluster. In contrast, the conventionally prepared materials contain mostly bimetallic and monometallic particles with variable compositions. The formation of smaller metal particles in the cluster-derived catalysts and the presence of the three metals in these particles in close proximity result in higher activity and selectivity for the hydrogenation of citral.

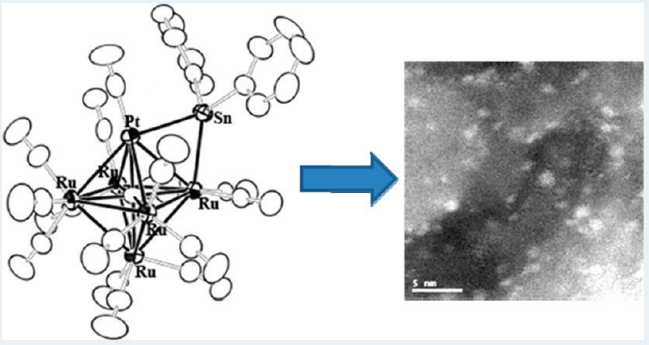

KEYWORDS: trimetallic catalysts, cluster-derived catalysts, Pt−Ru−Sn, citral hydrogenation

INTRODUCTION

Multimetallic catalysts frequently exhibit superior characteristics, including activity, selectivity, and stability, over their monometallic counterparts.[1] The term synergism has been advanced to describe this behavior[2] and has been attributed to ensemble, electronic, and bifunctional effects.[3,4] However, the method of synthesis of such multimetallic catalysts greatly affects the final structure and, hence, the catalytic properties. Conventional coimpregnation routes, for example, frequently result in the formation of monometallic nanoparticles on the catalyst surface with limited interactions between the constituent metals at the atomic level. As expected, such materials typically do not exhibit synergism during catalysis. In contrast, several studies have shown that heteropolynuclear cluster complexes can serve as highly effective precursors to supported catalysts with controlled multimetallic structure and composition at the nanoscale.[5−12] In turn, these catalysts frequently exhibit improved catalytic performance. Most of these efforts have focused on bimetallic systems, and only very few studies have investigated multimetallics, primarily because of the limited availability of such cluster precursors.

Supported Pt−Ru bimetallic catalysts are of interest to the catalytic community because of their stability under oxidizing and reducing atmospheres. Specifically, Pt−Ru clusters have been investigated as precursors for methanol oxidation electrocatalysts, yielding materials with narrower particle size distributions and higher activity when compared with commercially available catalysts.[13] Further, the addition of Sn to noble metal catalyst systems has been shown to improve performance, primarily by enhancing selectivity and preventing deactivation.[14,15] Hungria et al.[16] have recently shown that the addition of Sn to a Pt−Ru bimetallic system supported on mesoporous silica increased both activity and selectivity for the hydrogenation of dimethyl terephthalate to cyclohexanedimethanol.

In this work, we investigate the structural properties of trimetallic Pt−Ru−Sn catalysts prepared from a $PtRu_5(\mu\text{-}SnPh_2)(C)(CO)_{15}$ cluster precursor and compare them with catalysts of similar composition prepared by a conventional coimpregnation method. The cluster-derived catalysts were characterized by FTIR to monitor the carbonyl ligand removal process. The particle size distributions and metal particle compositions were also examined using high-resolution scanning transmission electron microscopy (HRSTEM) and energy-dispersive X-ray spectroscopy (EDS). Finally, the selective hydrogenation of citral (Figure 1) was used as a probe reaction for the characterization of the catalytic properties of the different materials. Thermodynamics favor the hydrogenation of the conjugated C═C bond over the C═O group during this reaction, although the opposite

Received: July 4, 2011
Revised: October 20, 2011
Published: October 27, 2011

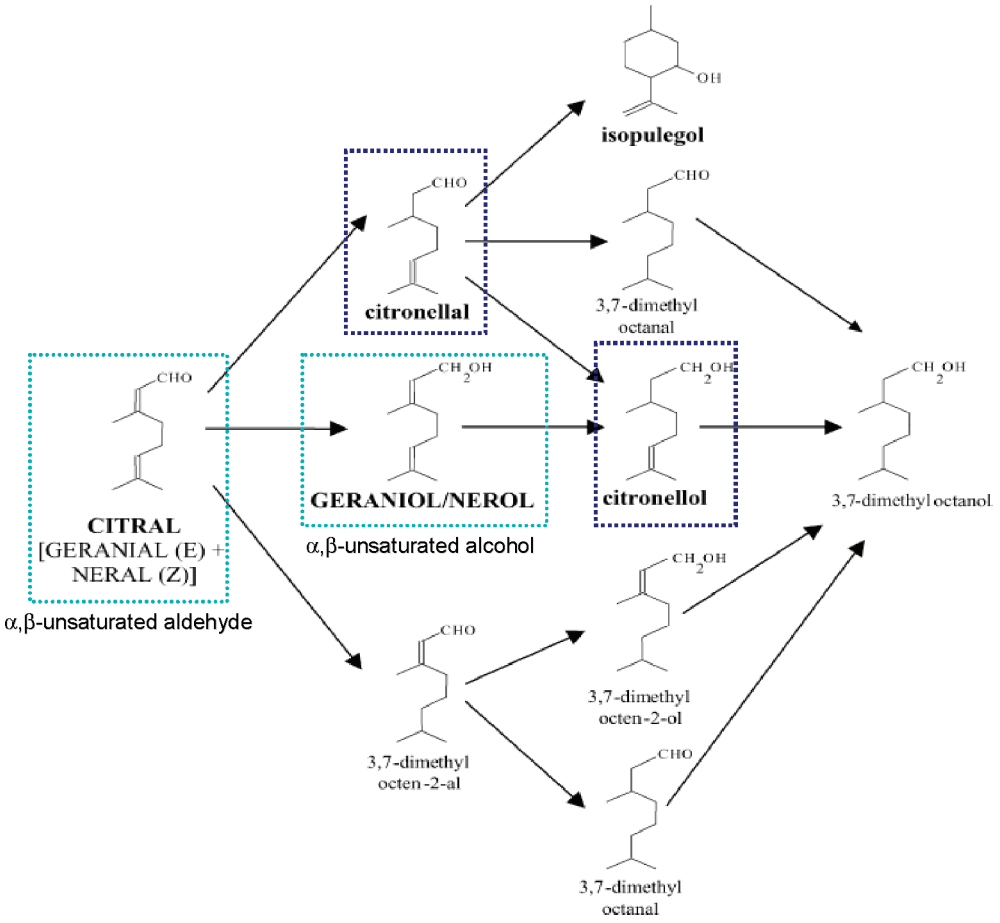

Figure 1. Reaction mechanism of the hydrogenation of citral.

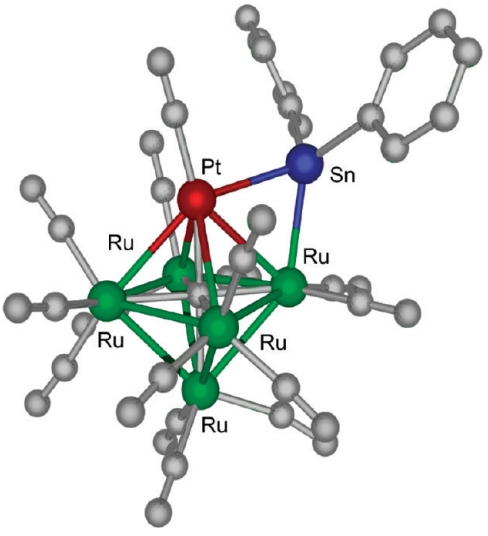

Figure 2. Ortep diagram of the cluster used as the precursor in this work.

is preferred from a practical standpoint, since it leads to the formation of the desired unsaturated alcohols (i.e., nerol and geraniol).[17] As a result, both activity and selectivity considerations are important when different catalysts are examined in this case.

EXPERIMENTAL PROCEDURES

Catalyst Preparation. The cluster precursor used in this work is the organometallic complex $PtRu_5(\mu\text{-}SnPh_2)(C)(CO)_{15}$, the synthesis of which was first reported by Adams et al.[18] The molecular structure of this cluster derived by single crystal X-ray diffraction analysis is shown in Figure 2. The Sn atom is coordinated to one Pt atom and one Ru atom, while the Pt atom is coordinated to four of the five Ru atoms. Three CO ligands are coordinated to each of the Ru atoms not associated with Sn, two CO ligands are coordinated to the Ru atom that is also coordinated to Sn, one CO ligand is coordinated to the Pt atom, and two phenyl ligands are coordinated to the Sn atom in the cluster.

Prior to impregnation, the MgO support (Sigma Aldrich 99+% purity, 325 mesh, 65 m^2/g,) was calcined at 773 K for 4 h. It was then pressed at 3500 psig into pellets that were subsequently ground and sieved to 60/80 mesh particles.

The solid $PtRu_5(\mu\text{-}SnPh_2)(C)(CO)_{15}$ cluster was kept in a dry nitrogen atmosphere at liquid nitrogen temperatures to preserve structural integrity. During catalyst preparation, the nominal amount of the cluster needed to achieve 0.4 wt % Pt, 1.0 wt % Ru, and 0.24 wt % Sn loading on MgO was dissolved in methylene chloride to form a deep red solution and added directly onto the MgO support contained in an amber round-bottom flask in a glovebox. The adsorption of the cluster on the support was immediate, as indicated by the MgO turning reddish

dx.doi.org/10.1021/cs2003559 |ACS Catal. 2011, 1, 1710–1718

pink and the methylene chloride becoming colorless. The addition of the cluster was done in the glovebox because of the short-term stability of the cluster in an oxidizing atmosphere. The flask was slowly stirred in a rotary evaporator in vacuo in the glovebox until the methylene chloride was completely evaporated. The resulting material was then stored inside the glovebox, where it was transferred to the appropriate reactor/cell as needed for subsequent treatments and measurements. All transfers and pretreatments were carefully conducted to prevent exposure to air.

$Pt(NH_3)_4(NO_3)_2$, $Ru(NO)(NO_3)_3$, and $SnCl_4.5H_2O$ precursors were used for the preparation of the conventional catalysts. The amounts of each precursor necessary to achieve 0.4 wt % Pt, 1.0 wt % Ru, and 0.24 wt % Sn loadings were added to water and then deposited on the MgO support by incipient wetness. After impregnation, the samples were dried in air at 393 K overnight and then stored in a N_2 atmosphere. Atomic absorption and inductively coupled plasma atomic emission spectroscopy (Galbraith Laboratories) analyses verified that both the cluster and metal-salt-derived catalysts used in all kinetic and chemical characterization experiments contain within analytical error the same weight loadings of Pt, Ru, and Sn, as reported above.

FTIR Characterization. Fourier transform infrared (FTIR) spectra of the trimetallic cluster and the MgO-supported cluster-derived catalysts were collected in the liquid and solid phases, respectively, using a Thermo Nicolet 7700 spectrometer with a resolution of 2 cm^{-1}. Each recorded spectrum is the average of 64 scans. For the liquid phase measurements, the cluster was dissolved in *n*-hexane and injected into a transmission FTIR cell equipped with NaCl windows and a path length of 0.5 mm. Solid MgO-supported samples of ~25 mg were pressed into wafers with a diameter of 12 mm. Calcined MgO was also pressed into a similar wafer and was used as the reference. The wafers were then mounted into a homemade, stainless steel transmission FTIR cell capped with NaCl windows. This cell can be heated to temperatures up to 773 K under gas flow. The cell was fitted with two sample holders, one in the sample beam and the other in the reference beam, so that the collected background/support spectrum could be subtracted from the catalyst wafer spectrum.

Samples were treated under 100 mL/min He flow overnight. The gas was then changed to 100 mL/min H_2 flow, and spectra were collected every 5 min over a 4 h period. The temperature of the sample was then ramped to 323 K at a rate of 8 K/min, with spectra still collected every 5 min. This ramping procedure was repeated every 50 K up to 673 K.

HRSTEM Characterization. Prior to HRSTEM measurements, all samples were treated in a tubular reactor according to the following protocol: heating in flowing H_2 from room temperature to 473 at 8 K/min; maintaining the temperature at 473 K under H_2 flow for 2 h; cooling to room temperature in flowing H_2 before purging with flowing N_2. A second series of identical samples were treated using a similar protocol with a high temperature of 573 K.

Approximately 100 mg of the treated catalyst was stored in N_2 and analyzed by HRSTEM. HRSTEM images were collected with a JEOL 2100F 200 kV microscope equipped with a CEOS C_s corrector in the illumination system. The geometrical aberrations were measured and controlled to provide less than a $\pi/4$ phase shift of the incoming electron wave over the probe-defining aperture of 15.5 mrad. High angle, annular, dark-field (HAADF) STEM images were acquired on a Fischione model 3000 HAADF detector with a camera length such that the inner cutoff angle of the detector was 50 mrad. The scanning acquisition was synchronized to the 60 Hz AC electrical power to minimize 60 Hz noise in the images, and a pixel dwell time of 16 μs was chosen. Metal particle diameters were measured using digital calipers and scaled to reflect their actual size, with 300 metal particles counted per sample. The surface weighted average particle size was then calculated as $\Sigma(n_i d_i^3)/\Sigma(n_i d_i^2)$, where n_i and d_i are the number of particles with a given diameter and the corresponding diameter, respectively. A solid-state Si(Li) X-ray detector from Oxford Instruments was used to collect the energy-dispersed X-ray spectroscopy (EDS) data. Although the imaging probe size is nominally 0.1 nm, the estimated probe size during EDS data collection was ~0.15 nm, with a probe current of 100 pA, as compared with 10 pA for the imaging probe. Quantification was carried out via Inca TEM software, which uses theoretical *k* factors for its thin-film microanalysis algorithm.

Citral Hydrogenation. Activity measurements were conducted in a 100 mL, EZE-Seal Autoclave Engineers reactor. Mass flow controllers were used to regulate the flows of N_2, O_2, and H_2 to the reactor, and a Spectra-Physics LC pump was used for the introduction of the liquid reactant mixture at reaction pressures up to 460 psig. The contents of the reactor were continuously stirred at a rate of approximately 1000 rpm, and a 4-way Valco valve permitted periodic liquid aliquot sampling of the reactor contents. The reactor was heated by a tightly clasped band heater, and the reaction temperature was monitored by a thermocouple mounted in a thermowell in the reaction medium. An HP5890 series II gas chromatograph (Supelco-wax column; FID detector) equipped with an autosampler was used to analyze reactant and products in the reaction mixture.

Prior to activity measurements, samples were treated as described in the HRSTEM section. A 500 mg portion of catalyst was added in the glovebox to the bottom housing of the autoclave reactor, already containing the dry isopropyl alcohol solvent. The bottom housing was then transferred from the glovebox and attached to the drive assembly of the reactor, with the isopropyl alcohol solvent serving as a protecting barrier to prevent exposure of the sample to air. An initial citral concentration of 0.167 M was used for all activity measurements, similar to what has been used in other citral hydrogenation studies.[19] The choice (isopropyl alcohol) and volume of solvent (60 mL), amount of catalyst (500 mg), reaction temperature (343 K), and pressure (460 psig) were also similar to those used in previous studies.[19−23] These similarities allow for the current results to be directly compared with those of the previous studies.

The reactor was sequentially flushed with flowing N_2 and H_2 at 1 bar pressure before being pressurized to 460 psig in H_2. Stirring at 1000 rpm was initiated next, and the temperature was raised to 343 K. A reactant solution containing 8 mL isopropyl alcohol, 2 mL citral, and 0.75 mL internal standard (diglyme) was then pumped into the reactor to mark the start of the reaction. Typically, 10−15 samples (<0.1 mL in volume) were taken over a period of 5 h during the course of each reaction and were analyzed off-line by injection via autosampler into the gas chromatograph. The samples were filtered by a 0.5 μm pore diameter frit assembly attached to the tip of the sampling tube inside the reactor so that the total catalyst amount in the reactor was maintained. To minimize the decrease in liquid volume, a four-way valve was used to back-flush liquid that remained in the sampling lines back into the reactor.

The autoclave reactor system was tested for the possible existence of both internal and external mass transfer limitations.

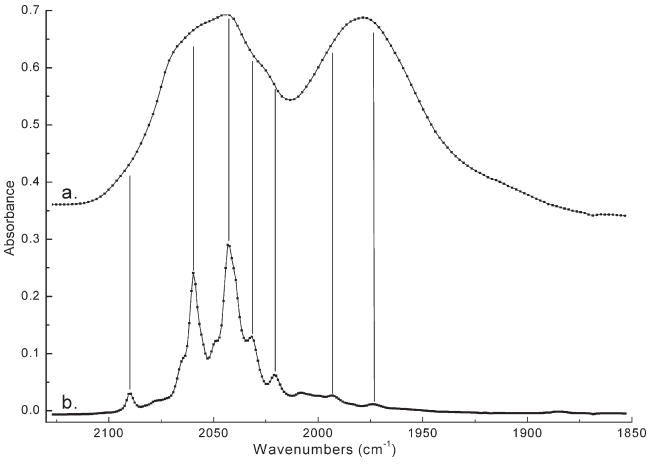

Figure 3. FTIR spectra of $PtRu_5(\mu\text{-}SnPh_2)(C)(CO)_{15}$ supported on MgO (a) and dissolved in hexane (b).

During these tests, the stir rate, catalyst particle size, and amount of catalyst were varied, and the initial rate constants obtained were all within an acceptable range of ±5%, indicating the absence of any mass transfer limitations in the reactor system. The material balance was also closely monitored to ensure that there were minimal discrepancies in the calibration of the analytical equipment. In all kinetic measurements, mass balances were closed to within 5%.

RESULTS AND DISCUSSION

FTIR Characterization. As indicated in the literature, the analysis of FTIR spectra of CO adsorbed on Ru surfaces can become fairly complicated because of the number of possible Ru oxidation states and types of adsorbed CO species formed.[24] In addition, the electronic state of Ru can be affected by the support. The three characteristic regions of high (2156−2130 cm^{-1}), medium (2100−2055 cm-^{1}), and low frequency bands (2092−1995 cm^{-1}) in such spectra are typically assigned to carbonyls adsorbed on Ru atoms with different oxidation states.[25] Even under conditions that should result in the full reduction of Ru^{n+} to Ru^0, CO peaks normally attributed to Ru^{n+}−CO species are still observed in the spectra because of the facile partial oxidization of surface Ru^0 atoms by disproportionation or dissociation of adsorbed CO.[26−31] The amount of literature examining the adsorption of CO on Ru is extensive and unambiguous. In this section, we will focus only on the literature addressing CO decomposition/desorption, since these are the processes taking place during the decarbonylation of the cluster precursor and the formation of the multimetallic particles on MgO in this study. For supported Pt particles, the linear CO stretching vibration is observed between 2050 and 2110 cm^{-1}, whereas for supported Pt carbonyl clusters, this stretching vibration is usually observed at frequencies below 2070 cm^{-1}.[32−42] In addition, for both supported Pt particles and supported Pt clusters, bridging CO vibrations are observed at ∼1850 cm^{-1}[37,39]

The FTIR spectrum for the $PtRu_5(\mu\text{-}SnPh_2)(C)(CO)_{15}$ cluster dissolved in hexane is shown in Figure 3 (spectrum b), with the different peaks present listed in Table 1; these peaks agree well with those observed in previously reported spectra[18] and confirm the purity of the cluster precursor used. The spectrum of the trimetallic cluster supported on MgO obtained in a H_2 atmosphere

Table 1. Bands Observed in the CO Stretching Region in the FTIR Spectra of the $PtRu_5(\mu\text{-}SnPh_2)(C)(CO)_{15}$ Cluster, As Well As Cluster-Derived $PtRu_5Sn$/MgO Samples Treated in H_2 at Different Temperatures

cluster dissolved in hexane (293 K)		$PtRu_5Sn$/MgO, H_2 treatment temperature (K)						
this work	literature[18]	293	323	373	423	473	523	573
			1915	1911	1901	1895	1885	1860
1973	1973	1978	1974	1972	1971	1967	1962	1944
1992	1992							
2021	2021	2025	2025	2025	2025	2023	2015	2005
2043	2043	2043						
2059	2060	2060						
2090	2090	2095						

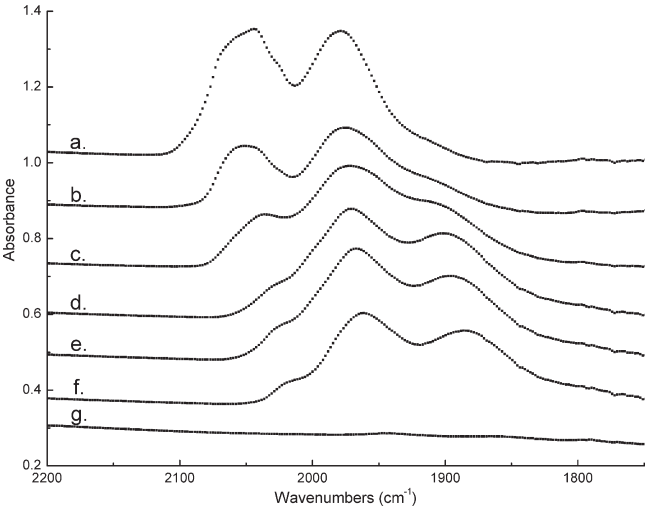

Figure 4. FTIR spectra of the $PtRu_5(\mu\text{-}SnPh_2)(C)(CO)_{15}$ cluster supported on MgO and treated in H_2 to (a) 293, (b) 323, (c) 373, (d) 423, (e) 473, (f) 523, and (g) 573 K.

at 293K is also shown in Figure 3 (spectrum a) with the positions of the peaks listed in Table 1. This spectrum presents certain similarities to the spectrum of the original cluster, although substantial broadening of the peaks between 1950 and 2000 cm^{-1} has also taken place. Others have also reported that FTIR spectra of Ru carbonyl clusters supported on MgO obtained at 293K include various broad carbonyl peaks in the 1850−2100 cm^{-1} range[31,43−46] and have attributed such broadening to a chemical shift of the CO ligands to more stable configurations, assisted by weak interactions of the CO groups with the MgO surface. As a result, the degree of broadening and, consequently, the exact position of the carbonyl peaks for the supported material depends on the calcination temperature of MgO, and hence, the degree of dehydroxylation,[43] since surface OH groups can behave as nucleophiles toward coordinated CO molecules. Removal of one or more CO ligands from either Ru or Pt and a subsequent shift of the remaining ligands to a more stable configuration also contribute to the appearance of new peaks, which combined with the existing ones, create the impression of further broadening in the spectra. It should be pointed out

dx.doi.org/10.1021/cs2003559 |ACS Catal. 2011, 1, 1710–1718

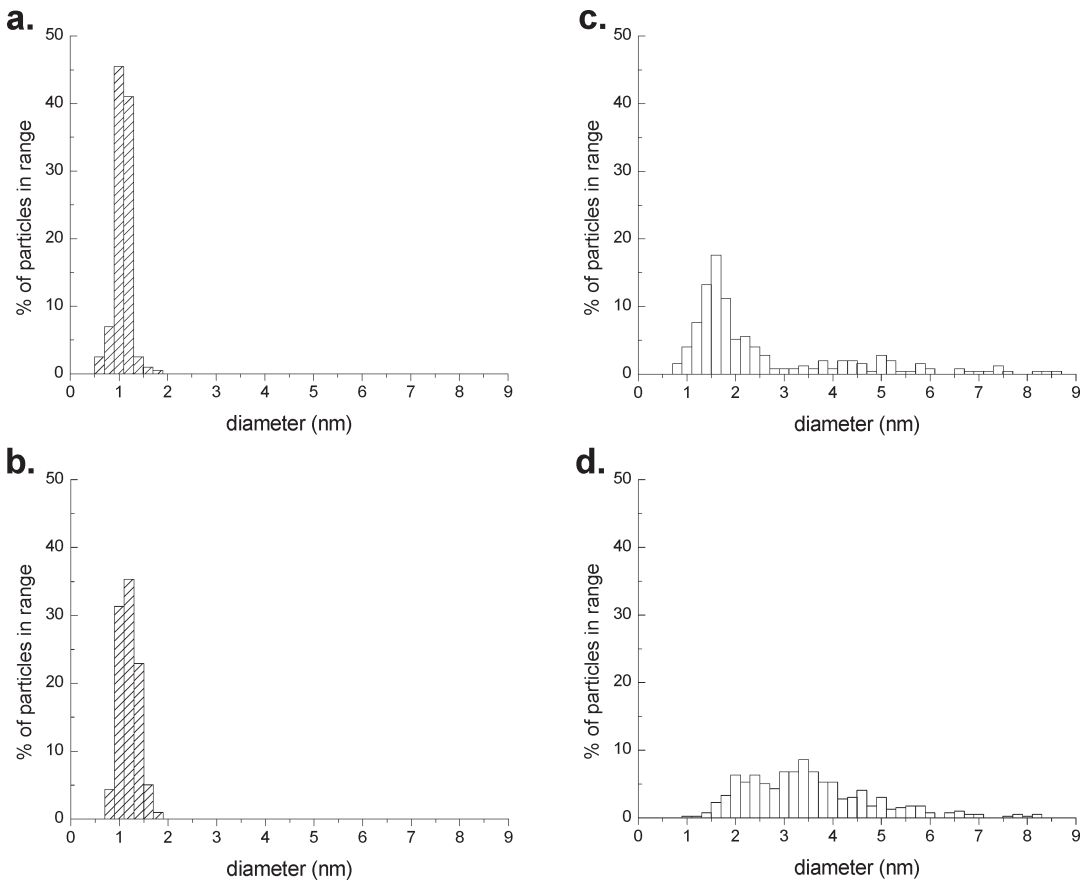

Figure 5. Particle size distributions for cluster-derived $PtRu_5Sn$/MgO samples pretreated at (a) 473 and (b) 573 K and conventionally prepared Pt−Ru−Sn/MgO samples pretreated at (c) 473 and (d) 573 K.

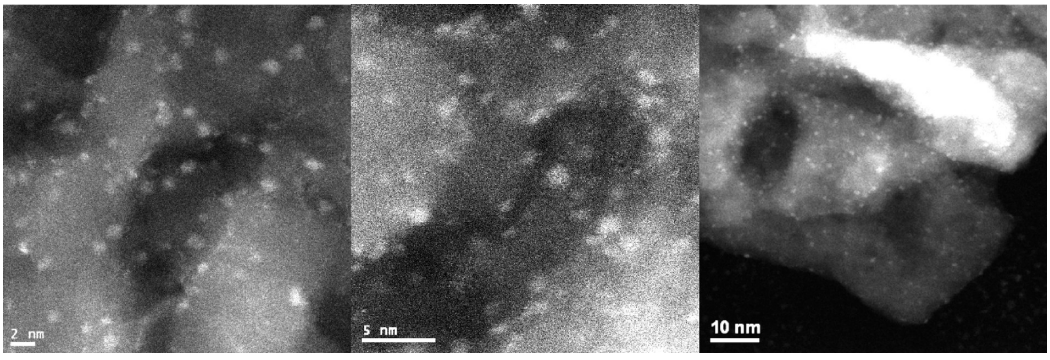

Figure 6. HRSTEM images at the 2, 5, and 10 nm scale of the cluster-derived $PtRu_5Sn$/MgO sample pretreated in H_2 at 473 K.

that without additional work, it is not possible to assign unambiguously all the peaks observed because of the several types of Ru carbonyls present, the similar frequencies of Ru and Pt carbonyls, and the relatively lower concentrations of the Pt carbonyls. Such work, however, is beyond the scope of the current manuscript.

No evidence was found in the 1560−1600 cm^{-1} region of the spectrum of the supported cluster for any phenyl C═C stretch associated with the two phenyl ligands in the original cluster, indicating that these ligands were most likely removed during the attachment of the cluster to the MgO surface. In agreement with this observation, Hungria et al.[16] previously suggested that the cleavage of the phenyl-Sn bonds allows this cluster to anchor on the surface of the support. They further pointed out that the presence of weak bonds between the phenyl ligands and Sn facilitates such anchoring, since the analogous cluster with Ge in the place of Sn that has much stronger phenyl-Ge bonds does not attach to the support.

Upon heating the MgO-supported cluster to 323 K (Figure 4, spectrum b), a new peak is observed at approximately 1900−1915 cm^{-1} (Table 1) and is likely due to an overlap of CO peaks coordinated to Pt and Ru (i.e., a bridging CO-Ru species or CO coordinated to Pt, both of which interact strongly with basic sites of the MgO support[31,44,47]). At the same time, the intensities of

dx.doi.org/10.1021/cs2003559 |*ACS Catal.* 2011, 1, 1710–1718

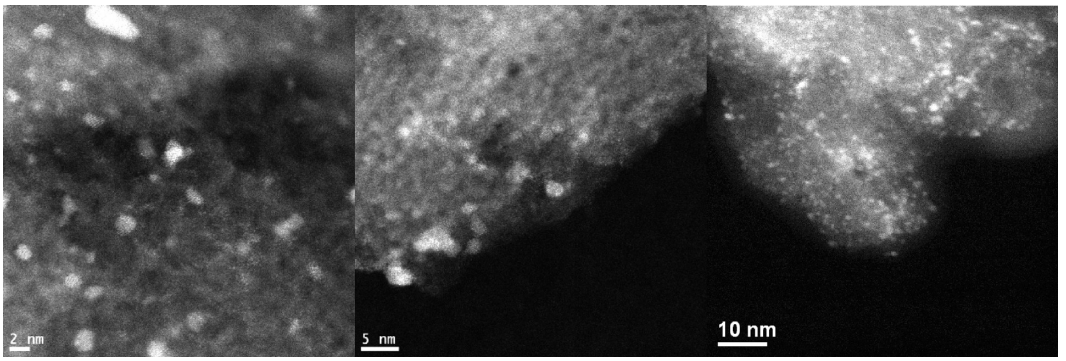

Figure 7. HRSTEM images at the 2, 5, and 10 nm scale of the conventionally prepared Pt−Ru−Sn/MgO sample pretreated in H_2 at 473 K.

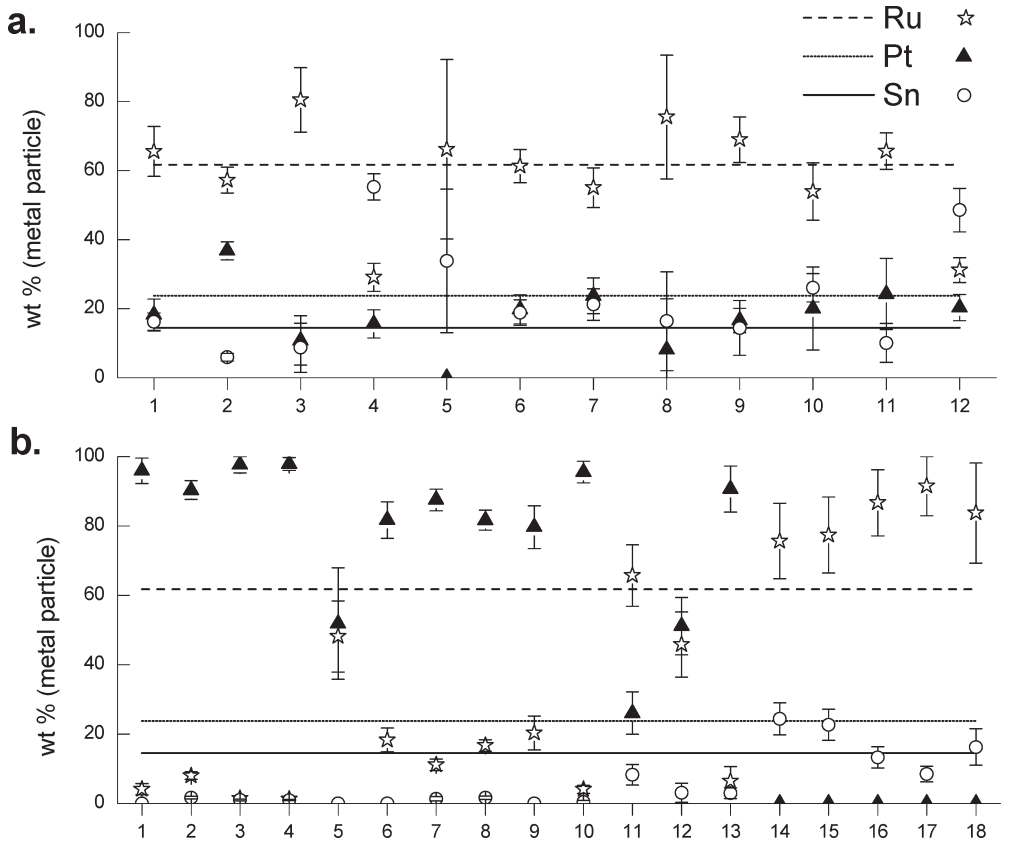

Figure 8. EDS measurements for several individual particles (numbered along the x axis) of the (a) cluster-derived $PtRu_5Sn$/MgO and (b) conventionally prepared Pt−Ru−Sn/MgO samples after pretreatment in H_2 at 473 K. Theoretical weight percent of the individual metals is shown by horizontal line markers.

the high-frequency peaks decrease substantially, while the intensities of the low frequency peaks increase and their positions shift to lower wavenumbers. These trends continue with further heating up to 523 K, and a final temperature increase to 573 K leads to the complete removal of CO from the surface (Figure 4, spectrum g). This is the most important result obtained from the FTIR measurements, since the scope of these measurements was to determine the temperature treatment needed for the removal of the carbonyl ligands from the supported cluster. Nevertheless, FTIR spectra obtained for the sample treated at 473 K following exposure to citral hydrogenation conditions show no evidence for the presence of any residual carbonyls. Thus, it appears that exposure to reaction conditions, particularly the H_2 pressures of 460 psig used in this reaction, can also complete the CO ligand removal process in situ during the use of these materials as catalysts.

Results similar to the ones observed in this study have been also reported by Guglielminotti et al.[31] during the decarbonylation of $Ru_3(CO)_{12}$ clusters supported on MgO, although in that work, experiments were conducted under vacuum, as opposed to the current use of flowing H_2 to purge the carbonyl groups from the surface. In both cases, the decrease in intensity of the peaks in the 1900−2040 cm^{-1} region indicates a loss of linearly bonded carbonyls on Ru. Such a loss is due to the desorption or reaction

dx.doi.org/10.1021/cs2003559 |*ACS Catal.* 2011, 1, 1710–1718

of some of these species as well as their conversion to more stable bridged structures with stretching frequencies below 1900 cm^{-1}. Similar results have also been obtained by Mizushima et al.[44] and Schwank et al.[45] during the desorption of CO from conventionally prepared Ru/MgO catalysts.

Structural Characterization. Particle size distributions of the four samples examined in this study were obtained by analysis of high resolution STEM images and are shown in Figure 5. Examples of the corresponding images of the trimetallic cluster-derived and conventionally prepared samples at the 2, 5, and 10 nm scale are shown in Figures 6 and 7, respectively. The results show significant differences in the average particle size and the particle size distribution, depending on the type of precursor used. A very narrow particle size distribution was observed for the cluster-derived samples with surface weighted average particle sizes of ~1.1 and 1.3 nm for the samples pretreated at 473 and 573 K, respectively. In contrast, the conventionally prepared samples exhibit much broader particle size distributions with surface weighted average particle sizes of 3.9 and 4.5 nm for the samples pretreated at 473 and 573 K, respectively. Although some sintering is indicated in both cases, the effect of the treatment temperature is rather small. Used samples were also analyzed in all four cases following citral hydrogenation. No appreciable changes in particle size were observed with the used samples for either the conventionally prepared or the cluster-derived catalysts.

EDS measurements conducted during HRSTEM analysis confirm the presence of trimetallic particles on the MgO surface after pretreatment of the cluster-derived sample in H_2 at 473 K. Metal ratios obtained for individual particles are similar to the atomic ratios of Pt, Ru, and Sn in the original cluster (Figure 8a) for the majority of the observed particles, suggesting that the clusters remained mostly intact following impregnation and thermal treatment in H_2. These results are in good agreement with similar results obtained from EDS studies by Hungria and Thomas for the same trimetallic cluster supported on a mesoporous silica support.[7,16] The average particle size of the cluster-derived catalysts is larger than the size of a single cluster and suggests that a few cluster units combine to form these particles. Such a model is consistent with our previous observations of other cluster-derived catalysts,[6,9−12] which indicate that while some cluster agglomeration takes place during impregnation and subsequent thermal treatments, no substantial metal segregation is apparent during this process, thus preserving the multimetallic character of the resulting supported nanoparticles. These nanoparticles are fairly uniform in terms of both size and metal composition. Pretreatment of the cluster-derived sample in H_2 at 573 K yields similar results, indicating that the 100 K difference in pretreatment temperature does not have a significant effect.

In contrast, the supported nanoparticles obtained through the conventional preparation approach exhibit a wide range of particle sizes and a varying degree of metal separation. EDS results (Figure 8b) for this sample show a large degree of heterogeneity in metal particle composition, with only a few trimetallic particles observed; within the spatial resolution of EDS, bimetallic Pt−Sn, Ru−Sn, and Pt−Ru particles are the prevailing species. In addition, several monometallic Pt particles were observed, mostly as large Pt aggregates, and Ru and Sn were observed only as bimetallic ensembles. EDS results further indicate that pretreatment at 573 K did not significantly affect the compositions of the supported nanoparticles obtained.

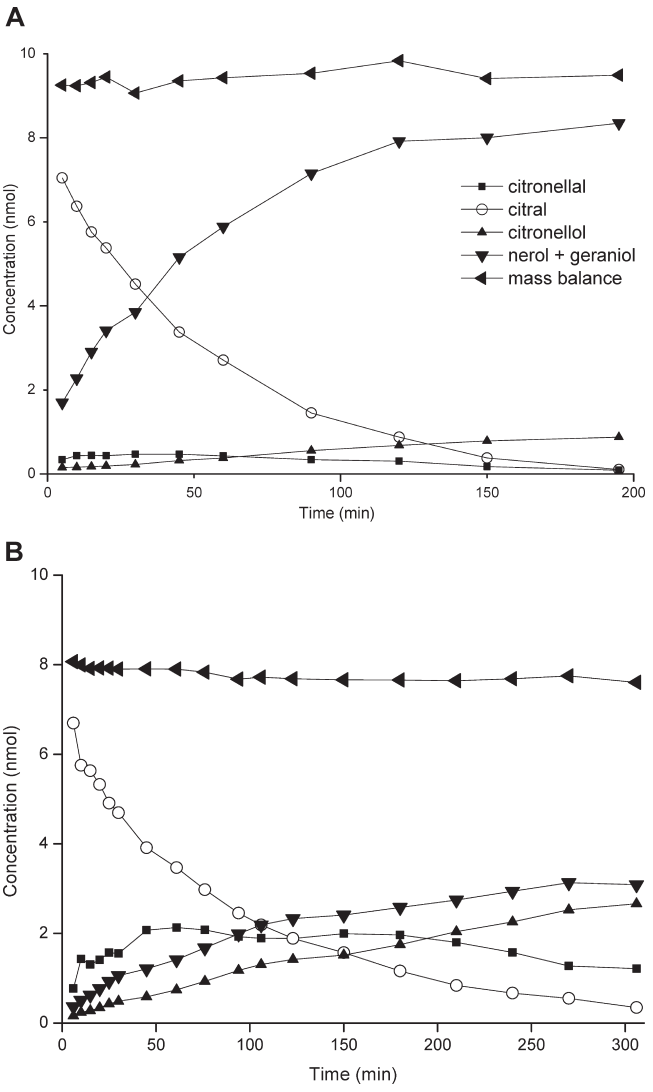

Figure 9. Normalized concentration profiles obtained during the hydrogenation of citral over the cluster-derived $PtRu_5Sn/MgO$ (a) and the conventionally prepared Pt−Ru−Sn/MgO (b) samples (○, citral; ▼, nerol and geraniol; ■, citronellal; ▲, citronellol; left-pointing triangle, overall mass balance; normalization was performed using the concentration of the internal diglyme standard).

Citral Hydrogenation. Examples of typical concentration profiles obtained during the hydrogenation of citral over the cluster-derived $PtRu_5Sn/MgO$ and the conventionally prepared Pt−Ru−Sn/MgO catalysts are shown in Figure 9. These results indicate that the cluster-derived catalyst is highly selective toward formation of the desired α,β-unsaturated alcohols: geraniol and nerol. The profiles also show that the concentration of citronellal goes through a broad maximum in concentration at ~50 min, consistent with the role of this species as an intermediate for the formation of citronellol (Figure 1). Finally, the observed concentration profiles indicate good overall closure of the mass balance.

Further analysis of the result of Figure 9 yields a first-order plot for the disappearance of citral under excess H_2 conditions (Figure 10). In fact, both catalysts studied exhibited first-order kinetics for citral disappearance. First-order kinetics under similar excess hydrogen conditions have also been observed for this reaction by several other authors using various monometallic

dx.doi.org/10.1021/cs2003559 |ACS Catal. 2011, 1, 1710–1718

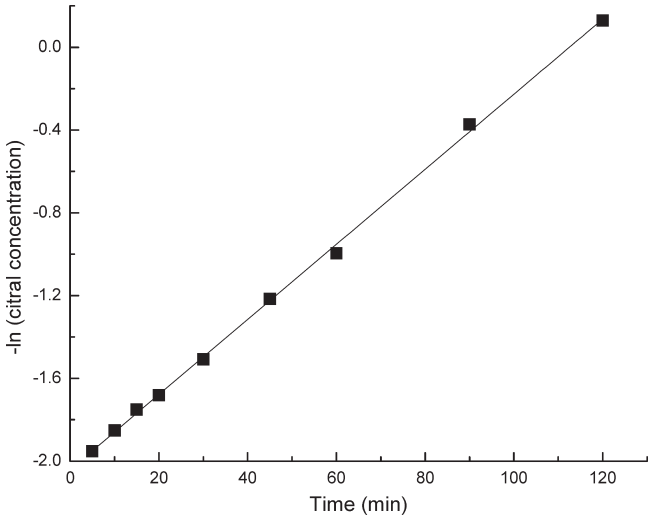

Figure 10. First-order kinetic plot for the citral concentration profile shown in Figure 9.

Table 2. Rate Constants, Percent Citral Conversion (C), Selectivity (S), and Yield (*Y* = CxS) to Unsaturated Alcohols (geraniol and nerol) after 30, 90, and 240 Minutes of Reaction over Cluster-Derived ($PtRu_5Sn$/MgO) and Conventionally Prepared (Pt−Ru−Sn/MgO) Catalysts

		30 min			90 min			240 min		
sample	*k*, (1/min*g metal)	C	S	Y	C	S	Y	C	S	Y
$PtRu_5Sn$	3.42	50	85	42	85	88	75	100	89	88
Pt−Ru−Sn	1.28	41	33	13	68	38	26	91	42	38

and bimetallic catalysts.[17,48] The first-order rate constants (calculated on the basis of the actual metal loadings), along with the selectivities and yields for the desired alcohol products (geraniol and nerol) at selected reaction times up to 100% conversion of citral for the samples examined are summarized in Table 2.

The results in Table 2 indicate that the type of precursor used greatly affects the catalytic performance of these materials. More specifically, the activity for citral hydrogenation and the selectivity to nerol and geraniol are substantially higher over the cluster-derived catalyst. Rate constants were normalized on the basis of total metal loading, since the trimetallic nature of the catalyst and our limited understanding of the types of active sites involved in the different reaction steps make it impossible to obtain site-specific rates (i.e., turnoever frequencies) at this point. The characterization results, however, clearly indicate that the cluster-derived catalyst has significantly smaller metal particles, which could easily account for the observed differences in activity.

The concentration profiles shown in Figure 9 suggest that the reaction proceeds over both cluster-derived and conventionally prepared catalysts through the same pathway (i.e., citronellal and geraniol/nerol are the first hydrogenation products, while citronellol is produced from these products in subsequent hydrogenation steps). Therefore, the observed differences in selectivity cannot be attributed to a change in the reaction pathway, but are rather associated with differences in the relative rates of competing reaction steps. Along these lines, it appears that the trimetallic nature of the supported particles in the case of the cluster-derived catalyst is very important, and the interactions between the three metal components apparently result in the suppression of the citronellal and citronellol reactions, leading to higher selectivities toward the desired geraniol and nerol intermediates.

CONCLUSIONS

Cluster-derived and conventionally prepared Pt, Ru, and Sn multimetallic catalysts of similar compositions have been prepared and characterized using FTIR, HRSTEM, and EDS. FTIR results indicate that under H_2 reduction conditions the ligands were partially removed in the cluster-derived catalysts at 473 K and then fully removed at 573 K. As the treatment temperature increased, the characteristic CO ligand peaks shifted to lower frequencies, indicating that stronger bridged bonds were being formed, similar to what was previously observed for supported Ru clusters. HRSTEM analysis shows that the cluster-derived catalysts exhibit significantly smaller average particle sizes (1.1 and 1.3 nm for catalysts treated at 473 and 573 K, respectively) than the corresponding conventionally prepared ones (3.9 and 4.5 nm for catalysts treated at 473 and 573 K, respectively). Particle size distributions indicate that the use of cluster precursors yields materials with very narrow particle sizes distributions, whereas conventionally prepared samples exhibit considerably broader distributions. Furthermore, EDS measurements show that in the cluster-derived catalysts, the supported metal nanoparticles are trimetallic in nature with composition similar to that of the original cluster. In contrast, EDS measurements indicate that the conventionally prepared sample contains mostly bimetallic and monometallic metal particles, with widely variable compositions. Finally, the cluster-derived sample exhibited substantially higher activity for citral hydrogenation and enhanced selectivity (90%) toward the desired unsaturated alcohols (nerol and geraniol) relative to the corresponding catalyst prepared using conventional methods (42%). Thus, it appears that the formation of smaller metal particles and the presence of the three metals in these particles in close proximity greatly improves both activity and selectivity for the formation of nerol and geraniol.

AUTHOR INFORMATION

Corresponding Author

*E-mail: amiridis@sc.edu.

REFERENCES

(1) Sinfelt, J. H. *Bimetallic Catalysts. Discoveries, Concepts and Applications*; Wiley: New York, 1983.
(2) Adams, R. D. *J. Organomet. Chem.* **2000**, *600*, 1.
(3) Rodriguez, J. A. *Surf. Sci. Rep.* **1996**, *24*, 223.
(4) Sinfelt, J. H. *Acc. Chem. Res.* **1977**, *10*, 15.
(5) Gates, B. C.; Lamb, H. H. *J. Mol. Cataly.* **1989**, *52*, 1.
(6) Siani, A.; Alexeev, O. S.; Captain, B. K.; Lafaye, G.; Marecot, P.; Adams, R. D.; Amiridis, M. D. *J. Catal.* **2008**, *255*, 162.
(7) Thomas, J. M.; Adams, R. D.; Boswell, E. M.; Captain, B.; Gronbeck, H.; Raja, R. *Faraday Discuss.* **2008**, *138*, 301.
(8) Thomas, J. M.; Johnson, B. F. G.; Raja, R.; Sankar, G.; Midgley, P. *Acc. Chem. Res.* **2003**, *36*, 20.
(9) Mihut, C.; Descorme, C.; Duprez, D.; Amiridis, M. D. *J. Catal.* **2002**, *212*, 125.
(10) Ortiz-Soto, L. B.; Alexeev, O. S.; Amiridis, M. D. *Langmuir* **2006**, *22*, 3112.
(11) Siani, A.; Captain, B. K.; Alexeev, O. S.; Stafyla, E.; Hungria, A. B.; Midgley, P. A.; Thomas, J. M.; Adams, R. D.; Amiridis, M. D. *Langmuir* **2006**, *22*, 5160.

(12) Siani, A.; Captain, B. K.; Adams, R. D.; Alexeev, O. S.; Amiridis, M. D. *Top. Catal.* **2011**, *54*, 318.
(13) Garcia, B. L.; Captain, B. K.; Adams, R. D.; Hungria, A. B.; Midgley, P. A.; Thomas, J. M.; Weidner, J. W. *J. Cluster Sci.* **2007**, *18*, 121.
(14) Galvagno, S.; Poltarzewski, Z.; Donato, A.; Neri, G.; Pietropaolo, R. *J. Mol. Catal.* **1986**, *35*, 365.
(15) Muraza, O.; Rebrov, E. V.; Berenguer-Murcia, A.; de Croon, M. H. J. M.; Schouten, J. C. *Appl. Catal., A* **2009**, *368*, 87.
(16) Hungria, A. B.; Raja, R.; Adams, R. D.; Captain, B.; Thomas, J. M.; Midgley, P. A.; Golovko, V.; Johnson, B. F. G. *Angew. Chem., Int. Ed.* **2006**, *45*, 4782.
(17) Gallezot, P.; Richard, D. *Catal. Rev.* **1998**, *40*, 81.
(18) Adams, R. D.; Captain, B.; Fu, W. *J. Organomet. Chem.* **2003**, *671*, 158.
(19) Lafaye, G.; Ekou, T.; Micheaud-Especel, C.; Montassier, C.; Marecot, P. *Appl. Catal., A* **2004**, *257*, 107.
(20) Silva, A. M.; Santos, O. A. A.; Mendes, M. J.; Jordao, E.; Fraga, M. A. *Appl. Catal., A* **2003**, *241*, 155.
(21) Giroir-Fendler, A.; Richard, D.; Gallezot, P. *Faraday Discuss.* **1991**, *92*, 69.
(22) Coupe, J. N.; Jordao, E.; Fraga, M. A.; Mendes, M. J. *Appl. Catal., A* **2000**, *45*, 45.
(23) Lafaye, G.; Micheaud-Especel, C.; Montassier, C.; Marecot, P. *Appl. Catal., A* **2002**, *230*, 19.
(24) Chin, S. Y.; Williams, C. T.; Amiridis, M. D. *J. Phys. Chem. B* **2006**, *110*, 871.
(25) Hadjiivanov, K. I.; Vayssilov, G. N. *Adv. Catal.* **2002**; *47*, 307.
(26) Yokomizu, G. H.; Louis, C.; Bell, A. T. *J. Catal.* **1989**, *120*, 1.
(27) Zanderighi, G. M.; Dossi, C.; Ugo, R.; Psaro, R.; Theolier, A.; Choplin, A.; D'Ornelas, L.; Basset, J. M. *J. Organomet. Chem.* **1985**, *296*, 127.
(28) Goodwin, J. G.; Naccache, C. *J. Catal.* **1980**, *64*, 482.
(29) Guglielminotti, E.; Boccuzzi, F.; Manzoli, M.; Pinna, F.; Scarpa, M. *J. Catal.* **2000**, *192*, 149.
(30) Hadjiivanov, K.; Lavalley, J.-C.; Lamotte, J.; Mauge, F.; Saint-Just, J.; Che, M. *J. Catal.* **1998**, *176*, 415.
(31) Guglielminotti, E. *Langmuir* **1986**, *2*, 812.
(32) Alexeev, O.; Graham, G. W.; Kim, D.-W.; Shelef, M.; Gates, B. C. *Phys. Chem. Chem. Phys.* **1999**, *1*, 5725.
(33) Hadjiivanov, K. I. *J. Chem. Soc., Faraday Trans.* **1998**, *94*, 1901.
(34) Stakheev, A. Y.; Shapiro, E. S.; Tkachenko, O. P.; Jaeger, N. I.; Schulz-Ekloff, G. *J. Catal.* **1997**, *169*, 382.
(35) Holmgren, A.; Andersson, B.; Duprez, D. *Appl. Catal., B* **1999**, *22*, 215.
(36) Hattori, T.; Nagata, E.; Komai, S.; Murakami, Y. *J. Chem. Soc., Chem. Commun.* **1986**, 1217.
(37) Anderson, J. A.; Rochester, C. H. *Catal. Today* **1991**, *10*, 275.
(38) Heyne, H.; Tompkin, F. C. *Trans. Faraday Soc.* **1967**, *63*, 1274.
(39) Boccuzzi, F.; Ghiotti, G.; Chiorino, A.; Marchese, L. *Surf. Sci.* **1990**, *233*, 141.
(40) Smolikov, M. D.; Zaitsev, A. V.; Khabibislamova, N. M.; Belyi, A. S.; Borokov, V.Yu,; Duplyakin, V. K.; Kazanskii, V. B. *React. Kinet. Catal. Lett.* **1994**, *53*, 169.
(41) Kubelkova, L.; Vylita, J.; Brabec, L.; Drozdova, L.; Bolom, T.; Novakova, J.; Shulz-Ekloff, G.; Gaelger, N. I. *J. Chem. Soc., Faraday Trans.* **1996**, *92*, 2035.
(42) Shen, J. G.-C. *J. Phys. Chem. B* **2000**, *104*, 423.
(43) D'Ornelas, L.; Theolier, A.; Choplin, A.; Basset, J.-M. *Inorg. Chem.* **1988**, *27*, 1261.
(44) Mizushima, T.; Tohji, K.; Udagawa, Y.; Ueno, A. *J. Am. Chem. Soc.* **1990**, *112*, 7887.
(45) Schwank, J.; Parravano, G.; Gruber, H. L. *J. Catal.* **1980**, *61*, 19.
(46) Bassi, I. W.; Garbassi, G.; Vlaic, G.; Marzi, A.; Tauszik, G. R.; Cocco, G.; Galvagno, S.; Parravano, G. *J. Catal.* **1980**, *64*, 405.
(47) Gandao, Z.; Coq, B.; Charles de Menorval, L.; Tichit, D. *Appl. Catal., A* **1996**, *147*, 395.
(48) Sokol'skii, D. V. *Kinet. Catal.* **1979**, *20*, 531.